Jones, T.A., and J. R. Mecikalski, 2023: Convective initiation forecasting using synthetic satellite imagery from the Warn-on-Forecast System. *J. Operational Meteor.*, **11** (10), 132-139, doi: https://doi.org/10.15191/nwajom.2023.1110.

Journal of Operational Meteorology
Short Contribution

Convection Initiation Forecasting Using Synthetic Satellite Imagery from the Warn-on-Forecast System

THOMAS A. JONES
Cooperative Institute for Severe and High-Impact Weather Research and Operations, University of Oklahoma, NOAA/OAR/National Severe Storms Laboratory, Norman, OK

JOHN R. MECIKALSKI
Atmospheric Science Department, University of Alabama in Huntsville, Huntsville, AL

(Manuscript received 13 December 2022; review completed 8 August 2023)

ABSTRACT

Forecasting convection initiation (CI) has advanced greatly during the past decade through the use of high-resolution satellite observations and model output. One of the primary CI products used in forecast operations is based on *GOES-16* visible and infrared imagery along with GLM lightning flash detections to determine the location of growing ice-containing cumulus clouds that are the precursor to developing thunderstorms. Another approach to CI forecasting that has recently become available is high frequency output from numerical weather prediction (NWP) models such as the Warn-on-Forecast System (WoFS). NWP model simulated composite reflectivity forecasts are one method used to determine when and where severe thunderstorms might develop. However, waiting for high reflectivity (> 40 dBZ) to be created within the NWP model limits the potential lead time available to forecasters when using WoFS output to anticipate areas where convection might form. Also, forecast reflectivity alone does not always give an indication of whether or not the precipitation developed by the NWP model is convective in nature. To address these limitations, this work applies a CI forecasting methodology developed for *GOES* satellite data on synthetic satellite imagery produced from WoFS output. Forecast cloud objects are tracked over a 10-min interval and CI forecasting parameters are applied to determine whether or not these cloud objects will continue to develop into organized thunderstorms.

1. Introduction

Convection initiation (CI) forecasting associated with high impact weather events is an important aspect of operational weather forecasting and remains a challenging topic. Many advances in CI forecasting have been made through the use of high resolution satellite data from the *GOES-R* series satellites. The Advanced Baseline Imager (ABI) onboard *GOES-R* measures Earth reflected and emitted visible and near-infrared/infrared (IR) radiation, respectively, which is influenced by atmospheric temperature, moisture, and cloud properties. One method to forecast CI is to measure the change in cumulus cloud properties over a short period of time (0-30 mins) to determine their likelihood of developing into thunderstorms during the next hour. Several CI forecasting algorithms have been developed to accomplish this task using various thresholding and/or regression techniques (e.g., Roberts and Rutledge 2003; Mecikalski and Bedka 2006; Mecikalski et al. 2010; Henderson et al. 2021; Leinonen et al. 2022). While the details among each algorithm differ, they all start by determining the location of growing cumulus clouds and creating cloud objects from those data. The cloud objects are then tracked over a period of time and changes in brightness temperatures (BTs) over various channels are determined. In many algorithms, CI requires that IR BTs (e.g., 10.3 μm) for a cloud object decrease as a function of time indicating that cloud tops are cooling because of an active updraft. Additional criteria relating to cloud depth and object size are also utilized (as described in section 3), as well as using various infrared, channel difference methods to assess cloud top altitude relative to the tropopause,

Corresponding author address: Thomas Jones, 120 David L. Boren Blvd, Norman, OK 73072
E-mail: Thomas.Jones@noaa.gov

and cloud-top glaciation. These algorithms have been developed and refined over the previous 15 years allowing for ongoing improvements in CI forecasting.

Recently, another tool for CI forecasting has been developed in the form of rapidly cycled NWP systems that generate high-frequency (e.g., 5 min) output over a regional domain in a real-time environment. One such system is the Warn-on-Forecast System (WoFS) developed by the National Severe Storms Laboratory in collaboration with the University of Oklahoma, Global Systems Laboratory, National Aeronautics and Space Administration, Storm Prediction Center, and National Weather Service partners (Stensrud et al. 2013; Wheatley et al. 2015; Jones et al. 2016, Skinner et al. 2018; Yussouf and Knopfmeier 2019; Jones et al. 2020; Gallo et al. 2022). The WoFS is a continually cycled ensemble data assimilation and forecasting system run daily over a moveable and flexible domain where high impact weather is expected. The resulting rain rate forecasts are one method that can be used to determine where convection is likely to occur. For the purposes of this work, convection is defined by an area of precipitation where radar reflectivity > 40 dBZ associated with clouds containing frozen hydrometeors indicating the presence of a buoyant updraft. One limitation of this method for assessing the convective potential is that any CI forecast made from WoFS output relies on the model generating precipitation, which is converted to simulated radar reflectivity for this application. It is also possible to create synthetic satellite imagery from the model output, which can show where cloud growth is occurring. Currently, this cloud growth is assessed in a qualitative manner and no objective method to determine the CI potential from this output exists. Recently, the capability to forecast lightning has been added to WoFS and it can represent where CI occurs. However, the current product generally requires hydrometeor concentrations corresponding to reflectivity > 40 dBZ; thus, providing little advantage over the reflectivity CI definition used here.

To address this forecast limitation, a modified version of the Mecikalski and Bedka (2006) and Mecikalski et al. (2015) CI algorithm is employed on 5-min resolution synthetic satellite imagery from WoFS to generate a probabilistic CI forecast parameter. Ice cloud objects will be tracked over a 10 min interval and assessed to determine whether or not they represent those that are likely to generate thunderstorms. In an operational environment, WoFS output is often viewed as products for each 5 min forecast interval. Given the current run-time of the system, a synthetic satellite-based CI forecasting product can provide a 5-10 min CI forecast advantage over waiting for WoFS reflectivity > 40 dBZ to be displayed. In addition, this product also distinguishes between whether or not developing precipitation is convective or stratiform in nature and whether or not lightning may occur. Both of these advantages can be important for increasing the forecast lead-time of high impact weather events as forecasters can begin preparations for advising the public on pending significant weather.

2. Warn-on-Forecast System

The WoFS is an ensemble-based NWP system to generate short-term (0-6 hour) probabilistic forecasts of high impact weather phenomena such as supercell updraft rotation, severe wind gusts, large hail, and heavy rainfall that may be conducive to flash flooding. The system has a horizontal grid spacing of 3 km and is initialized in the mid-morning using initial and boundary conditions from the 36 member High Resolution Refresh (HRRR) ensemble (Dowell et al. 2022; James et al. 2022). Conventional, WSR-88D radar reflectivity and radial velocity, and *GOES-16* cloud water path and clear-sky water vapor radiances, are assimilated at 15 min intervals for the duration of the event to continually update the cloud and precipitation fields in the model analysis. Boundary conditions are updated at hourly intervals. Forecasts are launched at 30 min intervals during the cycling process for the first 18 ensemble members, generating output at 5 min intervals. As of the summer of 2022, a 6 hour forecast takes ~40 mins to complete. The WoFS has been successfully used as part of the Hazardous Weather Testbed and in operations by the Storm Prediction Center and National Weather Service (Gallo et al. 2022). However, the WoFS value to CI forecasting has remained challenging by the time needed for >40 dBZ reflectivity to be forecast.

3. WoFS convection initiation product

The CI algorithm for *GOES* imager observations defined by Mecikalski and Bedka (2006) and Mecikalski et al. (2015) has been modified and applied to WoFS synthetic satellite imagery forecasts. Synthetic satellite imagery for each ensemble member and forecast time is generated by using the Radiative Transfer for the TIROS Operational Vertical sounder (RTTOV) model to translate the WoFS's members atmospheric state into

radiances (Saunders et al. 2018). For this work, the radiances are calculated using the coefficients generated for the *GOES-16* ABI. The process of calculating the CI product begins by classifying areas by clear, ice cloud (non or pre-convective), and other cloud types in each ensemble member (Fig. 1). Ice clouds are defined where model ice water path (IWP) is greater than 0.25 g kg^{-1} and 10.3 μm BT is less than 273.15 K. The IWP threshold was selected to remove non-convective thin cirrus areas from the CI forecast assessment. Cloud objects are generated from the convective cloud areas using the "SciPy" python package (Virtanen et al. 2020). The maximum search radius for a matched object is 18 km per 5 min interval. This radius is designed to take into account the shifting of centroid locations due to changing object characteristics in addition to movement from one time to the next. The minimum number of grid points per object is 4 and the maximum is 200. These criteria were selected to remove very small clouds (often a result of model noise) and mature storms from the cloud objects to be assessed for CI. Remaining cloud objects at a particular forecast time (t=0) are matched with those from the previous two forecast times (t –5, –10 min) and those which are matched at all three times are then assessed for potential CI. Cloud objects at the forecast time are classified as CI or non-CI objects based on a series of tests outlined in Fig. 1.

From Fig. 1, first, the mean of the five coldest 10.3 μm BT grid points for each matched object must decrease as a function of time by at least 6 K, consistent with cloud top cooling (Mecikalski and Bedka 2006). Second, the difference between the 6.2 μm and 10.3 μm channels ($BT_{62} - BT_{103}$) and between 13.3 μm and 10.3 μm channels ($BT_{133} - BT_{103}$) at t=0 must be less than –1 K. Both differences indicate that convective clouds are still growing and have not reached the tropopause and matured (Ackerman 1996; Schmetz et al. 1997; Ellrod 2004). Third, the difference in the 10 min trend of BT_{133} and BT_{103} must be less than –3 K, which also indicates that cloud top height is growing as a function of time. Finally, the size of the cloud object must increase during the 10 min period. Additional criteria were tested, but they did not provide any benefit to the set of tests already being used.

If all criteria are reached for a particular cloud object, a binary true/false CI parameter for those grid points encompassing that object is set to 'true'. Once the CI parameter has been calculated for each ensemble member at a particular forecast time, the probability of CI is determined by the proportion of members

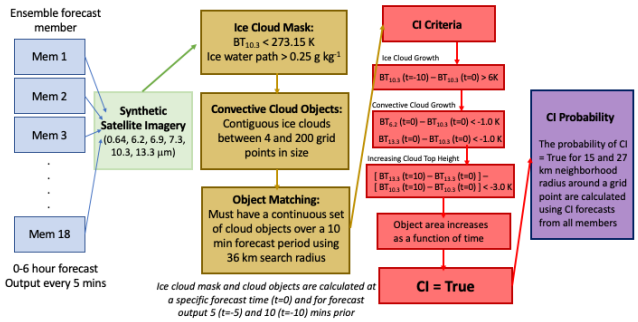

Figure 1. Flowchart for the WoFS CI algorithm using synthetic satellite forecast output. *Click image for an external version; this applies to all figures hereafter.*

that satisfy the CI parameter for 15 or 27 km diameter neighborhoods surrounding a grid point (Schwartz and Sobash 2017). Probabilistic CI plots are then generated at each forecast time starting at 10 mins after the initialization time for display to forecasters. No smoothing is applied to the plots at this time.

4. Forecast results

The WoFS CI product was tested on several spring 2022 high impact weather days. Two examples from 29 April and 10 May 2022 are provided to assess its potential to improve CI forecasting. For 29 April, a set of ensemble forecasts was initiated at 1900 UTC at which time ongoing precipitation was occurring in western Nebraska (NE), while evidence of developing convection was beginning to occur in western Kansas (KS). At 1930 UTC, simulated BT103 30 min forecast imagery from one ensemble member shows both features (Fig. 2a). By 1940 UTC, BT103 associated with the clouds in KS have noticeably cooled compared to 1930 UTC, indicating strengthening convection in the model (Fig. 2c). Applying the convective cloud mask highlights the location of the growing ice-clouds (Fig. 2d-f). Convective cloud objects are then defined, and are shown in Fig. 2 (g-i). Note that the ice clouds associated with the ongoing NE precipitation (denoted by "X") are not considered potential CI objects. The remaining objects in KS denoted at "A" and "B" grow in size between 1930 and 1940 UTC. At 1940 UTC, the CI algorithm for this ensemble member is triggered for the largest two objects in KS (Fig. 2i).

The same method is applied to all ensemble members, and Fig. 3 shows the probability of CI within 15 and 27 km neighborhoods at 1940 UTC. An area of CI probability > 30% is forecast in a region in western

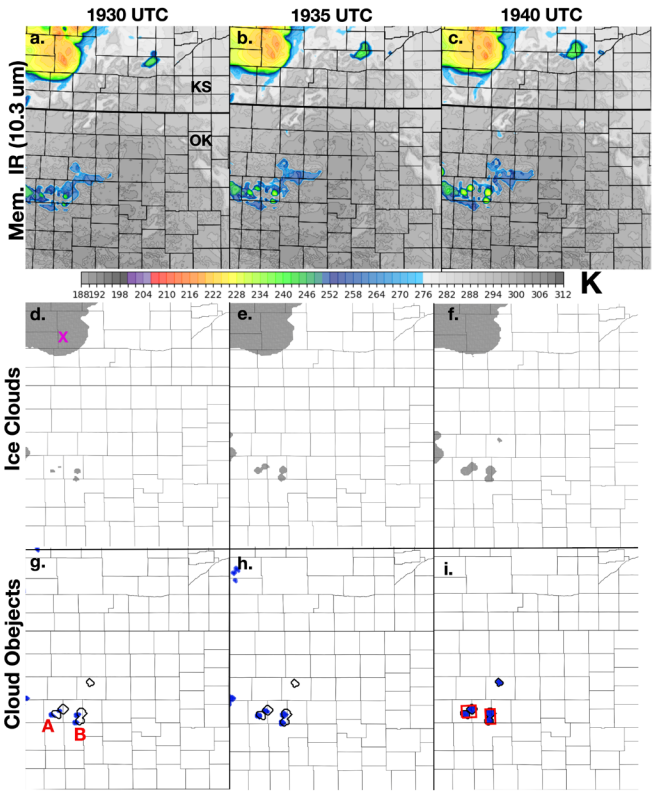

Figure 2. Synthetic satellite BT103 imagery from member 10 of a WoFS forecast initiated on 1900 UTC 29 April 2022 valid at 1930 (a), 1935 (b), and 1940 UTC (c). Ice cloud areas at the same forecast time (d, e, f) and convective cloud objects that satisfy the conditions for potential CI objects at each forecast time (g, h, i). Red squares denote that the CI algorithm has been triggered for those particular objects. Outlines of 1940 UTC cloud objects (t=0) in the CI algorithm are provided on the 1930 and 1935 UTC images for comparison.

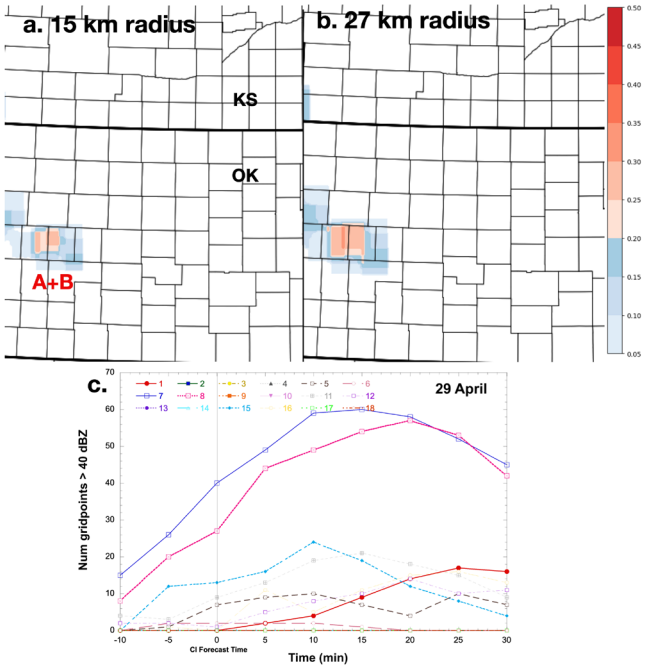

Figure 3. Probability of CI = true for 15 (a.) and 27 km (b.) neighborhoods valid at 1940 UTC for forecasts initiated at 1900 UTC 29 April 2022. Areas where probability exceeds 30% are indicative of where CI is likely in this system. The number of forecast grid-points where composite reflectivity is > 40 dBZ for each ensemble member in the area where CI is forecast for that member at t=0 (1940 UTC) from 10 minutes prior to the CI forecast until 30 mins afterward (c.). Bold line indicates the member described in Fig. 2.

KS using the 27 km neighborhood (Fig. 3b). This plot indicates that approximately one-third of the 18 ensemble members contain CI objects in this area at 1940 UTC. The larger the neighborhood size, the more likely high probability areas will be defined, at the cost of a greater uncertainty in forecast CI location. The performance of each member can be tracked by calculating the number of forecast composite reflectivity grid-points > 40 dBZ within the CI area from a period 10 minute prior to a valid CI forecast to 30 minutes after (Fig. 3c). At 1940 UTC, a total of 9 members forecast CI somewhere in the domain. Some members, including the one described above (mem 8), already have > 40 dBZ grid-points present, while others do not. In six members, the number of > 40 grid points in the CI area increases in the following 15 mins. Afterward, precipitation moves out of the original CI area, and the number decreases.

Overall testing of this system over four separate events indicated that CI probabilities between 30-50% represented strong signals for future CI. Since the early phases of convection are often not analyzed by the model, spread in forecast CI is often large (Guerra et al. 2022). Thus, it is extremely difficult or uncommon for CI probabilities to reach values in excess of 50% at a particular location. It should also be noted that the CI probabilities remain low nearby the mature thunderstorms in NE, due to cloud object size exceeding the algorithm limit (Fig. 1). This is a positive result since the goal of this product is to highlight where convection will develop, not where it already exists.

The usefulness of this product is determined by whether or not it indicates that precipitation is likely to develop based on the model ensemble, and if it will be convective in nature prior to it being displayed to forecasters in the existing WoFS product suite. Currently, WoFS displays reflectivity "paintballs" from

each member where forecast composite reflectivity is > 40 dBZ. As a result, the CI forecast would be considered a success if a high probability of CI existed before the 40 dBZ threshold has been exceeded. Figure 4 (paintballs a,c) shows the contours of reflectivity > 40 dBZ for each ensemble member at 1940, 1955, and 2010 UTC. At 1940 UTC, the existing precipitation in NE is well forecast by most members. Further south, only three members generate > 40 dBZ at this time (Fig. 4a). By 1955 UTC, the number of members with convection has increased significantly with a corresponding increase in coverage (Fig. 4b). The increasing trend continues as shown in the 2010 UTC forecast (Fig. 4c). Forecast composite reflectivity from ensemble member 8 during this period also shows increased intensity and coverage. However, it should also be noted that a small area of composite reflectivity > 40 dBZ already exists at the 1940 UTC forecast with the western CI object, indicating that the product's lead-time might be small in some cases (Fig. 4d-f). Overall, the CI forecast is generally consistent with observations with an area of Multi-Radar / Multi-Sensor (MRMS) reflectivity > 35 dBZ located in western KS at 1940 UTC, which grows into precipitation with reflectivity > 55 dBZ by 2010 UTC (Fig. 4g-i). There is a small displacement error between the maximum CI probabilities and observed CI, but the timing and general region are consistent.

Another example of this CI product is shown for 40 min forecasts initialized at 1900 UTC on 10 May 2022 in southwestern TX. Between 1930 and 1940 UTC several areas of existing and growing convection are evident from BT_{103} imagery (Fig. 5a-c) and a large thunderstorm is already forecast in northern Mexico at 1930 UTC. A growing convective cell is also present in far southwest TX during this period and defined as cell "A". Further north, areas of mid-to-upper level ice clouds are forecast over a large region. However, close inspection shows two areas of significant cloud cooling, defined as cells "B" and "C". Applying the ice-cloud mask highlights these areas along with some of the other ice-cloud features (Fig. 5d-f). The non-convective ice-cloud features such as "X" and "Y" are removed when determining the location of convective cloud objects with cells A, B, and C now clearly evident (Fig. 5g-i). At 1940 UTC, the CI parameters are met for A, B, and C indicating that CI is likely in these areas. In the case of cell "A", the very cold cloud tops at 1930 UTC indicate convective precipitation is already ongoing. This object lies on the edge of the growth-size criteria in the CI algorithm, and by 1945 UTC, the CI parameter is

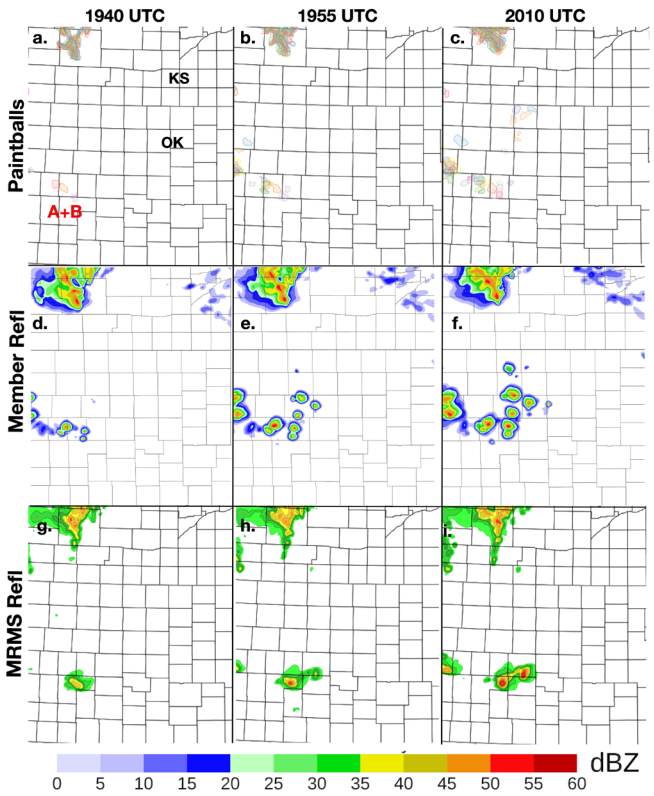

Figure 4. Areas of forecast composite reflectivity > 40 dBZ for all ensemble members at 1940 (a), 1955 (b), and 2010 UTC (c) with each ensemble member represented by a different color. Corresponding member 10 forecast reflectivity at these times (d, e, f) along with observed MRMS reflectivity at these times (g, h, i).

no longer triggered (not shown). The other two objects are much smaller and appear pre-convective in nature.

The probabilistic CI forecasts valid at 1940 UTC for the 15 and 27 km neighborhoods show two areas of CI probabilities > 30%, which are associated with cells "B" and "C" (Fig. 6). A third area exists along the TX – Mexico border, but note that the CI probability associated with cell "A" is rather low. For cells "B" and "C", the CI algorithm is triggered for several members and most do not have convection in these areas at 1940 UTC. The 40-dBZ paintball plots at this time show only two members with convection near cell "B" and only one near cell "C" (Fig. 7a). Only a single member forecasts reflectivity > 40 dBZ corresponding to cell "A", which happens to be the member shown above. This is evident on the probabilistic plots in Figure 6 as one large square of 5% probability at this location, with a slightly higher value in the southwest corner of this square. Twelve members forecast CI within this domain at 1940 UTC and for nine members including

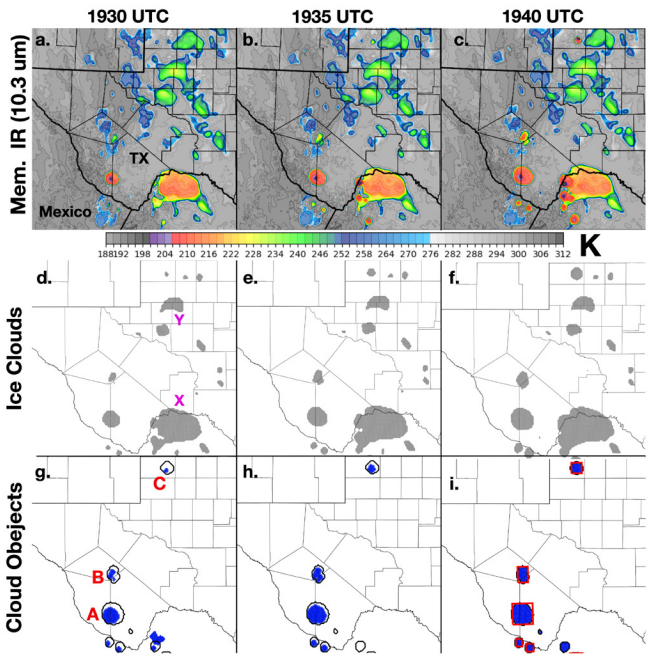

Figure 5. As in Fig. 2, but for 1930, 1935, and 1940 UTC ensemble member 6 synthetic satellite imagery, ice clouds, and CI objects for a forecast initiated at 1900 UTC 10 May 2022. For this case, individual storm objects of interest are denoted as "A", "B", and "C".

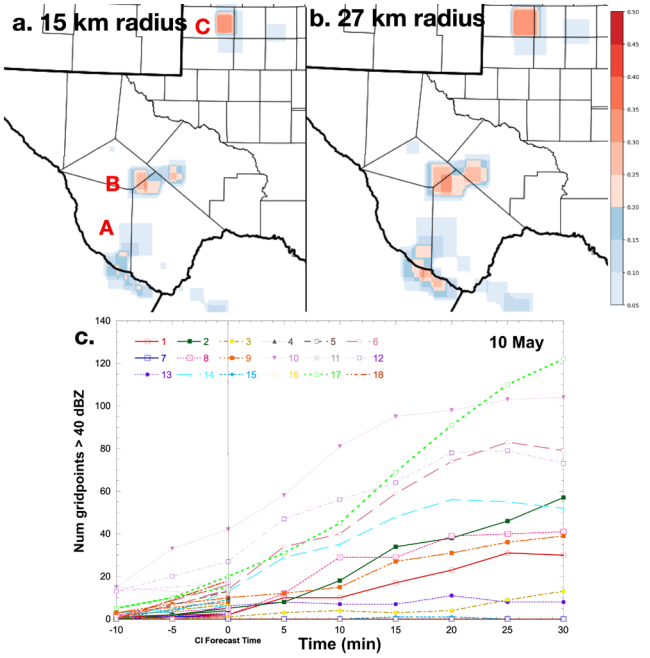

Figure 6. As in Fig. 3, but for 10 May 2022, and the member described in Fig. 5.

the one described above (mem 2) (Fig. 6c). For these members, the number of forecast grid-points > 40 dBZ with the CI areas increases during the following 30 min period.

Composite reflectivity forecast for this time shows cell "A" to be well on its way to development, with "B" and "C" showing increasing reflectivity values with "B" already having a small area of reflectivity > 40 dBZ (Fig. 7d). Also forecasted are several areas of non-convective precipitation between cells "B" and "C", which are correctly not identified by the CI forecast. By 1955 UTC, many more ensemble members forecast convection associated with cells "B" and "C", with some development further south, but displaced from cell "A" (Fig 7b, d). By 2010 UTC, most members are forecasting convection associated with "B" and "C" indicating that the CI forecast was accurate when compared against forecast reflectivity. Observed MRMS reflectivity between 1940 and 2010 UTC shows convective development in these two areas with 40 dBZ reflectivity being present with cell "B" at 1955 UTC and cell "C" at 2010 UTC (Fig. 7g-i). In both cases, the forecast and observations line up quite well. Also of note is that the MRMS observations also show a developing storm roughly corresponding to cell "A". This indicates that even low-probability forecast events may still occur.

5. Conclusions

The WoFS-based CI nowcast product was developed, and demonstrated using four severe weather cases occurring in April - May 2022, and two examples described here (29 April and 10 May) show the potential of this product as well as its limitations. As for the two other cases, WoFS substantially over-forecasted thunderstorms for one (2 May), and the other (31 May) performed very similarly to the 10 May case. The goal of this product is to both improve the lead-time for potential CI forecasting within WoFS and also compared to observations. The focus of this work is on the first goal, with future work focused on a more complete verification once the CI has matured through additional testing. The initial product generally highlighted areas where forecast convection was forming and in its early development stages. False alarms associated with mature thunderstorms and non-convective precipitation were low. For the 29 April example, the lead-time between the probability of CI exceeding 30% and a similar number of members generating areas of composite reflectivity > 40 dBZ was only 10-15 mins. In practical terms, this corresponds to only a 2-3 min lead-time in the displayed forecast product. Recall that

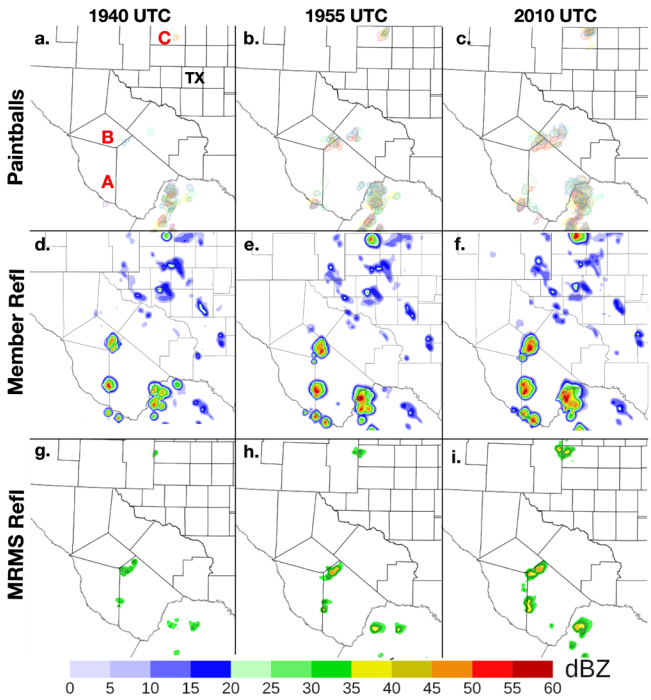

Figure 7. As in Fig. 4, but for 10 May 2022.

forecast images are displayed as they are generated and a lead-time of 15 min corresponds to three images, which are created every 1-2 min. The 10 May example performed somewhat better, with slightly longer CI lead-times. Lead time relative to severe convection was much larger (> 1 hour) as the first severe weather reports associated with the CI related storms did not occur until after 2100 UTC. For all cases, the probabilistic CI product was most effective in the 0-2 hour portion of the forecast period. Afterward, the ensemble spread becomes too large for CI probabilities much above 10% to be generated.

One major limitation of this product is that a significant number of ice-hydrometeors must be generated by the model prior to being identifiable on synthetic satellite imagery. Generally, high ice-hydrometeor production corresponds to the model already resolving a significant convective storm updraft, with precipitation already occurring. Thus, the potential forecast lead time is lower (~15 min) in this system than with *GOES* satellite-based observations. One potential remedy is a higher resolution model. Tests of a 1-km WoFS showed a longer period between the first ice-hydrometeors being generated and precipitation being observed. Choices in the model cloud microphysics schemes are also likely to impact lead-time and further tuning of these schemes may be required. Ideally, this would increase the lead time closer to the 30 min period, which is where we believe the product would have its greatest impact. Overall, the results showed promise and continued refinement is underway. It is expected that this product will be generated in real-time during upcoming Hazardous Weather Testbeds.

Acknowledgments. This research was funded in part by the NOAA Warn-on-Forecast project. Additional funding was provided the under the NOAA-University of Oklahoma Cooperative Agreement NA21OAR4320204, U.S. Department of Commerce. HRRR ensemble initial and boundary conditions for this work were provided by the Global Systems Laboratory as part of ongoing real-time experiments. We also thank Dr. Patrick Skinner for his review of the initial draft and the valuable comments he provided.

REFERENCES

Dowell, D. C., and Coauthors, 2022: The High-Resolution Rapid Refresh: An hourly updating convection-allowing forecast model. Part 1: Motivation and system description. *Wea. Forecasting*, **37**, 1371-1395.

Gallo, B., K. Wilson, J. Choate, K. Knopfmeier, P. Skinner, B. Roberts, P. Heinselman, I. Jirak, and A. Clark, 2022: Exploring the Watch-to-Warning Space: Experimental Outlook Performance during the 2019 Spring Forecasting Experiment in NOAA's Hazardous Weather Testbed. *Wea. Forecasting*, **37**, 617-637, https://doi.org/10.1175/WAF-D-21-0171.1.

Guerra, J. E., P. S. Skinner, A. J. Clark, M. Flora, B. Matilla, K. Knopfmeier, and A. E. Reinhart, 2022: Quantification of NSSL Warn-on-Forecast System accuracy by storm age using object-based verification. *Wea. Forecasting*, **37**, 1973–1983.

Henderson, D., J. Otkin, and J. Mecikalski, 2021: Evaluating Convective Initiation in High-Resolution Numerical Weather Prediction Models Using *GOES-16* Infrared Brightness Temperatures. *Mon. Wea. Rev.*, **149**, 1153 – 1172, https://doi.org/10.1175/MWR-D-20-0272.1.

James, E. P., and Coauthors, 2022: The High-Resolution Rapid Refresh (HRRR): An hourly updating convection-allowing forecast model. Part 2: Forecast performance. *Wea. Forecasting*, **37**, 1397-1417.

Jones, T. A., K. Knopfmeier, D. Wheatley, G. Creager, P. Minnis, and R. Palikonda, 2016: Storm- scale data assimilation and ensemble forecasting with the NSSL experimental Warn-on- Forecast system. Part II: Combined radar and satellite data experiments. *Wea. Forecasting*, **31**, 297–327.

Jones, T. A., P. Skinner, N. Yussouf, K. Knopfmeier, A. Reinhart, X. Wang, K. Bedka, W. Smith Jr., R. Palikonda, 2020: Assimilation of *GOES-16* Radiances and Retrievals into the Warn-on-Forecast System. *Mon. Wea. Rev*, **148**, 1829–1859.

Leinonen, J. U. Hamann, U. Germann, and J. R. Mecikalski, 2022: Nowcasting thunderstorm hazards using machine learning: the impact of data sources on performance. *Nat. Hazards Earth Syst. Sci*., **22**, 577–597.

Mecikalski, J. R., and K. M. Bedka, 2006: Forecasting convective initiation by monitoring the evolution of moving convection in daytime *GOES* imagery. *Mon. Wea. Rev*., **134**, 49–78.

Mecikalski, J. R., W. M. MacKenzie Jr., M. König, and S. Muller, 2010: Cloud-Top Properties of Growing Cumulus prior to Convective Initiation as Measured by Meteosat Second Generation. Part II: Use of Visible Reflectance, *Journal of Applied Meteorology and Climatology*, **49** (12), 2544-2558.

Mecikalski, J. R., J. K. Williams, C. P. Jewett, D. Ahijevych, A. LeRoy, and J. R. Walker, 2015: Optimizing use of geostationary satellite observations and the development of probabilistic 0–1hour convective initiation nowcasts. *Journal of Applied Meteorology and Climatology*, **54**, 1039-1059.

Roberts, R. D., and S. Rutledge, 2003: Nowcasting storm initiation and growth using *GOES-8* and WSR-88D data. *Wea. Forecasting*, **18**, 562–584.

Schwartz, C. S., and R. A. Sobash, 2017: Generating probabilistic forecasts from convection-allowing ensembles Using neighborhood approaches: A review and recommendations. *Mon. Wea. Rev*, **145**, 3397-3418. https://doi.org/10.1175/MWR-D-16-0400.1

Skinner, P. S., and Coauthors, 2018: Object-based verification of a prototype Warn-on-Forecast system. *Wea. Forecasting*, **33**, 1225–1250.

Saunders, R., J. and Coauthors, 2018: An update on the RTTOV fast radiative transfer model (currently at version 12), Geosci. Model Dev., 11, 2717–2737, https://doi.org/10.5194/gmd-11-2717-2018

Stensrud, D.J., and Coauthors, 2013: Progress and challenges with Warn-on-Forecast. Atmos. Res., 123, 2–16, https://doi.org/10.1016/j.atmosres.2012.04.004.

Virtanen, P., and Coauthors, 2020: SciPy 1.0: Fundamental algorithms for scientific computing in Python. *Nat Methods*, **17**, 621-272.

Wheatley, D. M., K. H. Knopfmeier, T. A. Jones, and G. J. Creager (2015), Storm-scale data assimilation and ensemble forecasting with the NSSL Experimental Warn-on-Forecast System. Part I: Radar data experiments. *Wea. Forecasting*, **30**, 1795–1817.

Yussouf, N. and K. H. Knopfmeier (2019), Application of Warn-on-Forecast System for Flash-Flood Producing Heavy Convective Rainfall Events, *Quart. J. of Royal Meteor. Soc*., **145**, 2385–2403, https://doi.org/10.1002/qj.3568.